Classification of Galactograms with Ramification Matrices: Preliminary Results[1]

Predrag R. Bakic, PhD, Michael Albert, PhD, Andrew D. A. Maidment, PhD

Rationale and Objectives. The poor specificity of galactography, the imaging modality generally indicated in cases of nipple discharge, has led to a large number of biopsies with negative results. A quantitative scheme for classifying galactographic findings might help reduce the number of such biopsies in the future. As a first step toward that goal, the authors have studied one quantitative method for describing the branching of ducts by using ramification matrices (R matrices), and the correlation of the values of the matrix elements with clinical findings.

Materials and Methods. The ductal trees were manually segmented for 25 galactographic views from 15 patients, and corresponding R matrices were calculated. Patients were divided into two groups: those with no reported galactographic findings (NF) and those with reported findings (RF) of ductal ectasia, cysts, or papilloma. In a leave-one-out fashion, the authors evaluated a classification scheme that was based on R-matrix coefficients and used a Bayesian decision rule. The effects of segmentation were tested by successively removing each of the terminal ducts and computing the corresponding matrices of the pruned trees.

Results. With use of a single R-matrix element, 92% and 62% of NF and RF cases were correctly classified, respectively ($P = .007$). With use of two elements, 83% and 77% of NF and RF cases were correctly classified, but this result was not statistically significant ($P = .108$). In a test of robustness, an analysis of pruned trees yielded an average root-mean-square fractional difference of 9.7% between the elements of the original and the R matrix averaged over all pruned trees.

Conclusion. The preliminary analysis indicates that it may be possible to identify cases with reported galactographic findings by using R matrices.

Key Words. Breast, ducts; breast neoplasms, diagnosis; galactography.

Virtually all breast cancers derive from epithelial tissue, with 90% of malignant lesions arising in the ductal epithelium (1, p 118). Most carcinomas spread initially along the lumen of the ducts or lobules. Evidence of this growth pattern is seen in the distribution of calcifications associated with early breast cancer, which often follows the ductal pathway (2).

Major ducts of the breast extend from the nipple toward the chest wall in a branching network of smaller and smaller ducts, which defines a draining territory, or lobe (1,3–6). The adult breast contains 15–20 irregular lobes, which converge to the nipple. Each lobe is drained by its own major duct. Several major ducts merge to form an ampulla (or lactiferous sinus), a dilated segment beneath the nipple. Branching of the ducts toward the chest wall continues until a duct finally ends in blunt fingerlike ductules formed by the acini, the basic glandular secretory units. During lactation the ductal network drains milk

Acad Radiol 2003; 10:198–204

[1] From the Department of Radiology, Thomas Jefferson University, Suite 3390 Gibbon Bldg, 111 S 11th St, Philadelphia, PA 19107-5563. Received September 6, 2002; revision requested October 16; final revision received and accepted November 7. Supported by U.S. Department of Defense, grant DAMD-17-98-1-8169. **Address correspondence to** A.D.A.M.

produced in the acini. Ductules surrounded by specialized connective tissue are called *lobules*. A lobule with its terminal duct is known as the *terminal ductal lobular unit*.

Some cancers are revealed by nipple discharge alone, with no palpable or mammographic lesions. Indicated in cases of nipple discharge, galactography is a procedure for imaging the contrast material–enhanced ductal network (7–9). It is performed by carefully identifying the discharging nipple orifice, introducing a blunt needle, and injecting a small amount of radiographic contrast material. Pre- and postcontrast mammograms are obtained with the needle in place, thereby revealing the breast lobe that contains the discharging duct. Various ductal patterns (eg, filling defects, ductal ectasia) can be recognized from galactograms (10). Galactography lacks specificity (1), a situation that results in a large number of biopsies with normal or benign results. A quantitative radiographic classification scheme for galactograms might help reduce the percentage of biopsies with negative results and the related psychological and economic effects.

The ductal origin of breast cancer is the physiological basis for various techniques of diagnosis and treatment. The analysis of nipple aspirate fluid (11) has been investigated for early cancer detection. Breast cancer risk has been estimated by analyzing the parenchymal pattern of projected fibrous and ductal structures (12). In surgical assessment of nipple discharge, preoperative staining of the ducts can minimize the amount of tissue excised (9). The breast ductal network has been modeled by tracing the points of duct entrance to and exit from a series of subgross histologic slices (13,14). The use of statistical analyses of ductal networks for breast modeling also has been reported (15,16).

Describing the normal ductal network is difficult because of anatomic variability and low radiographic contrast. Here, we report a method of analyzing ductal networks by using ramification matrices (R matrices), which describe the topologic shape of a treelike structure (17). The R-matrix elements represent branching probabilities at various levels of a tree and can be used to describe a given tree or to generate a family of trees. The probabilistic nature of R matrices makes them useful for generating many individual synthetic trees with matching statistical properties of branching. For this reason, R matrices have been used to generate ductal networks in breast modeling for mammographic simulation (16).

The morphology of the ductal network reflects the state of breast development and the healthy or pathologic state of the breast tissue, as has been shown by analyses of the branching of murine mammary ducts in different phases of gland development (18,19) and by studies of epithelial cellular organization under the influence of hormones, growth factors, and carcinogens (20–22). We hypothesize that diseases of the breast, demonstrated through alterations of the normal ductal anatomy, can be quantified and classified from galactograms. In the present study, we manually segmented ductal trees from 25 galactograms, calculated the R matrices, and computed the probability of correct classification for a combination of R-matrix elements. We also tested the robustness of the R-matrix representation by analyzing pruned trees.

MATERIALS AND METHODS

Clinical galactograms for this analysis were obtained retrospectively from 15 patients with a mean age of 49.2 years (range, 29–75 years). These patients were selected from a group of 41 who had undergone galactography at the Thomas Jefferson University Breast Imaging Center, Philadelphia, Pa, during the 6½-year period from June 1994 through January 2001. Galactograms from 17 of the 41 patients were unavailable because they had been returned to the patients or the primary health care institutions, and galactograms from another nine patients were not used, because of obstruction or poor image quality (ie, the complete ductal tree could not be segmented). Of the 15 patients whose cases were analyzed, eight (mean age, 44.2 years; range, 29–74 years) had no reported galactographic findings (hereafter NF), and seven (mean age, 54.8 years; range, 43–75 years) had galactographic findings of ductal ectasia, cysts, or papilloma (hereafter RF). Twenty-five galactographic views of the 15 patients were analyzed (16 craniocaudal [CC] and nine mediolateral or mediolateral oblique [hereafter denoted in combination as ML/MLO]), of which 12 views (eight CC and four ML/MLO) were from NF cases and 13 (eight CC and five ML/MLO) were from RF cases. There were no reported findings of malignancy from these 25 galactograms. Furthermore, mammographic follow-up data were available for eight of the 15 patients for an average period of 4.75 years (range, 3.5–6.0 years), and no malignancies were reported. Patients' ages, available galactographic views, symptoms, and reported galactographic findings are listed in the Table.

To reconstruct the ductal topology, each branch in the ductal network was drawn by hand on a sheet of tracing paper placed over the galactogram displayed on a light box (Figure 1). The points where ducts branched were

Patient's Age, Available Views, Symptoms, and Galactographic Findings

Age (y)	View	Symptom	Galactographic Finding
29	LCC	Greenish discharge	None
30	LML, LCC	Clear/yellow discharge	None
32	LML(Mag), LCC	Bloody discharge	None
36	LCC	Bloody/yellow discharge	None
43	RML, RCC	Greenish discharge	Cysts
44	RCC	Bloody discharge	Cysts, ductal ectasia
45	RCC, LML	Bloody/milky discharge	None
45	LCC	Dilated ducts on mammogram and US image	None
47	RMLO, RCC RML, RCC	Greenish discharge, mastitis	Cysts, ductal ectasia
50	RML, RCC	Greenish discharge	Cysts
55	RCC, RMLO	Clear discharge	Cysts
63	LMLO, LCC	Darkish discharge	None
70	RCC	Bloody discharge	Ductal ectasia
74	LCC	Clear/bloody discharge	None
75	RCC	Bloody discharge	Papilloma

Note.—LCC = left craniocaudal, LML = left mediolateral, RML = right mediolateral, RCC = right craniocaudal, RMLO = right mediolateral oblique, LMLO = left mediolateral oblique, and Mag = magnified.

distinguished from the points of overlap by the fact that the latter are galactographically brighter, due to superposition of the x-ray attenuation. Large ducts were reconstructed by connecting the marked points. In each of the segmented ductal trees, the root, internal and terminal nodes, and branches were labeled and the R-matrix elements were computed as described by Viennot et al (17). Simplified, the algorithm is given as follows: (*a*) all terminal branches have label 1, (*b*) a "parent" branch whose "children" have labels i and j will be labeled by $\max(i, j)$ if $i \neq j$ or by $(i + 1)$ if $i = j$, and (*c*) the labeling procedure continues until the root branch is reached whose label s is called the *Strahler number* of the tree structure.

The R matrix of a tree with Strahler number s is a lower triangular matrix, defined as

$$R_{(s-1),s} = [r_{k,j} = b_{k,j}/a_k,\ k \in (2, s),\ j \in (1, k)], \quad (1)$$

where a_k is equal to the number of branches with label k (17). For $j < k$, $b_{k,j}$ is the number of pairs of branches with labels k and j, while for $j = k$, $b_{k,j}$ is the number of pairs of branches both labeled $k - 1$, descending from a node. Therefore, $r_{k,j} = b_{k,j}/a_k = p(b_{k,j}|a_k)$ is the probability that a branch with label k will bifurcate into branches with the appropriate labels. Figure 1c shows the numerically labeled branches of the segmented ductal tree from Figure 1a. In Figure 1c, there are 14 branches with label 2, six of which bifurcate into pairs of branches with labels 1 and 2, corresponding to the probability of $r_{2,1} = 6/14 = 0.43$. The other eight branches with label 2 bifurcate into pairs of branches both with label 1, corresponding to the probability of $r_{2,2} = 8/14 = 0.57$. In a similar manner, all the elements of the R matrix shown in Figure 1d were computed from the galactogram shown in Figure 1a. We computed R matrices with nine elements and Strahler number $s = 4$, corresponding to a root branch with label 4.

A linear Bayesian decision rule was used to classify the galactographic findings. In the design of the Bayesian classifier, we assumed that the data were normally distributed and that the population standard deviation was the same for both classes. These assumptions reduce the risk of overspecification due to the small sample size. We estimated the standard error of the classification results by means of a leave-one-out (jackknife) method, in which the percentages correctly classified are calculated for subsets of the data formed by leaving each sample out in turn. The standard error of the classification results is then the standard deviation of the values calculated for the jackknife subsamples (23).

A preliminary test of the robustness of the R-matrix approach was performed by analyzing pruned ductal trees derived from an original tree after removal of a single terminal branch. This test was proposed because of the observed ambiguity in tracing terminal branches, which can be easily overlooked due to their small size and low

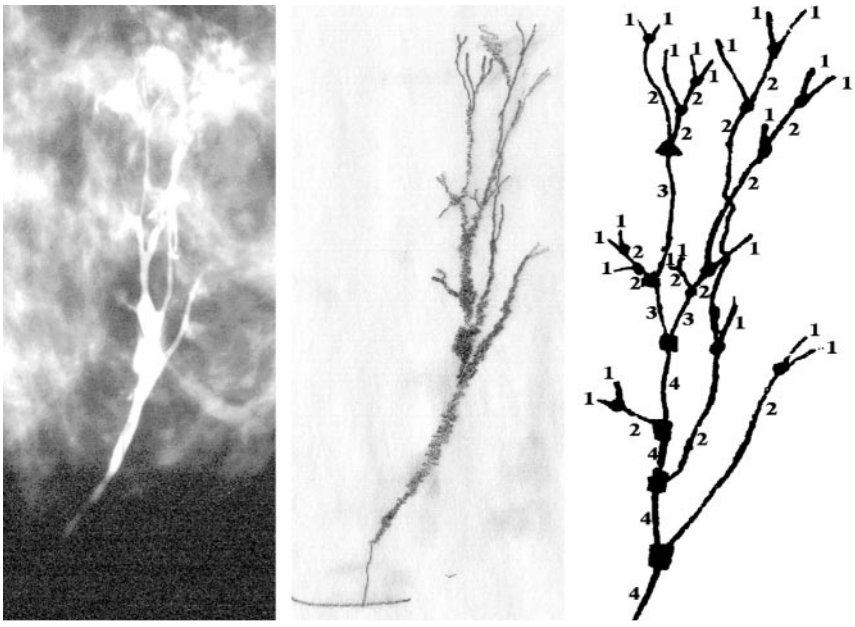

$$R = \begin{bmatrix} r_{2,1} & r_{2,2} & . & . \\ r_{3,1} & r_{3,2} & r_{3,3} & . \\ r_{4,1} & r_{4,2} & r_{4,3} & r_{4,4} \end{bmatrix} = \begin{bmatrix} 0.43 & 0.57 & . & . \\ 0 & 0.33 & 0.67 & . \\ 0 & 0.75 & 0 & 0.25 \end{bmatrix}$$

d.

Figure 1. Segmentation of a ductal tree, showing **(a)** part of a galactogram with a contrast–enhanced ductal network, **(b)** the manually traced network of larger ducts from the contrast–enhanced portion of the galactogram, **(c)** numeric labeling of branches in the ductal network, and **(d)** the R matrix computed from the branching pattern. The dots, triangles, and squares denote branching points of different levels of the tree.

contrast. Consequently, some of the terminal branches might have been omitted, resulting in a pruned version of the original tree. The R matrix of a pruned tree was computed and the procedure was repeated for each of the terminal branches in the original tree. A comparison was performed by computing the root-mean-square fractional difference, as follows:

$$D = \sqrt{\sum_{k=2}^{s} \sum_{j=1}^{k} \left[\frac{r_{k,j} - r_{k,j}^{\text{prun}}}{r_{k,j}} \right]^2 / N_{\text{el}}}, \qquad (2)$$

where $r_{k,j}$ and $r_{k,j}^{\text{prun}}$ are the elements of the original R matrix and the matrix averaged over all pruned versions of the original tree, respectively. N_{el} is the number of nonzero R-matrix elements ($N_{\text{el}} \leq 9$ for $s = 4$, from Eq [1]).

RESULTS

The values of the R-matrix elements calculated from clinical galactograms and the averages over all NF and all RF cases are plotted in Figure 2. Some matrix elements show a noticeable difference in mean value between the two classes (eg, $r_{3,2}$ and $r_{3,3}$), suggesting the possibility of classifying galactographic findings on the basis of R matrices. We evaluated a classification scheme that used either a single matrix element or a pair of them and a linear Bayesian decision rule in a leave-one-out fashion. The classification performance of a single R-matrix element was best (in terms of the sum of the correctly identified fractions in the two groups) for $r_{3,3}$, which correctly classified 92% ± 2 of NF and 62% ± 3 of RF cases. In a combination of two elements, $r_{3,2}$ and $r_{3,3}$ correctly classified 83% ± 4 of NF cases and 77% ± 4 of RF cases. Figure 3 illustrates the classification results.

To estimate the statistical significance of the classification results, we performed an additional experiment by using random numbers as descriptive parameters. Six numbers, corresponding to the linearly independent elements of the R matrix with nine elements, were randomly generated for each of the 25 galactograms. This procedure was repeated for 10,000 trials, and in each trial the ran-

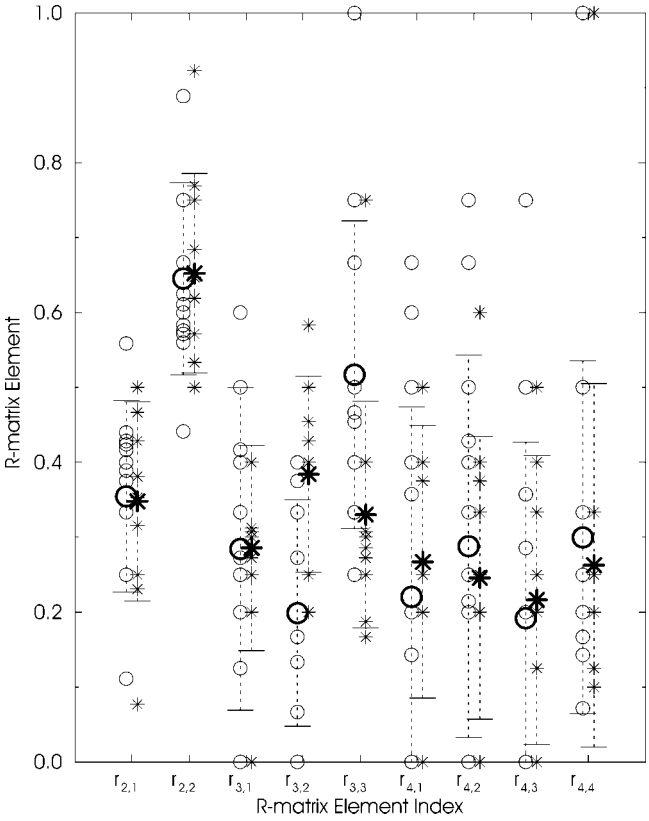

Figure 2. Values of the R-matrix elements. Bold symbols (○ = RF, ∗ = NF) represent element values averaged over all RF and all NF cases, and light symbols represent the individual cases. Error bars correspond to the sample standard deviations.

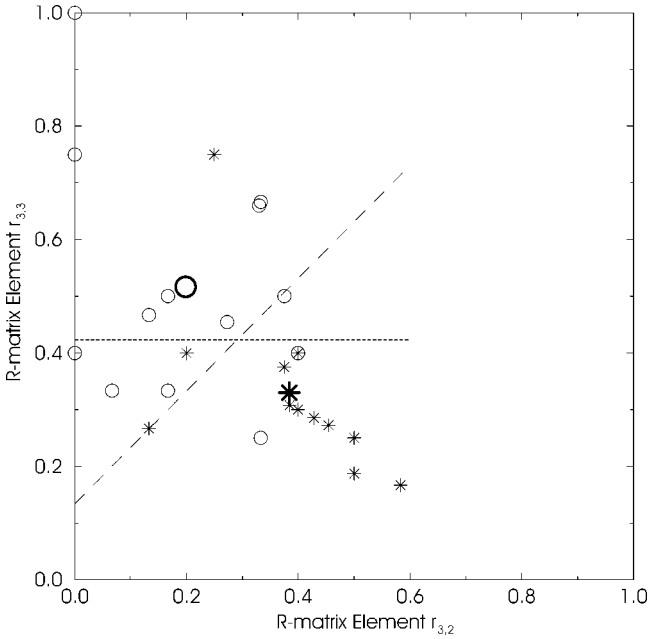

Figure 3. Classification of galactographic findings based on elements of the R matrix and a Bayesian linear decision rule. Bold symbols (○ = RF, ∗ = NF) represent element values averaged over all RF and NF cases, and light symbols represent the individual cases. Short dashes indicate Bayesian decision line for $r_{3,3}$, and long dashes indicate Bayesian decision line for $r_{3,2}$, $r_{3,3}$.

domly generated data were used to classify galactograms by means of either one or two matrix elements, as was done for the real data. In 0.7% of trials, one of the parameters showed a classification power of at least 92% for one class and at least 62% for the other—comparable with the performance of element $r_{3,3}$ on the clinical galactograms. Thus, if the classification result observed for the clinical galactograms is by chance alone, it would be encountered in just 0.7% of repeated experiments, and the statistical significance for classification with $r_{3,3}$ is $P = .007$. The classification results achieved with the pair of elements $r_{3,2}$ and $r_{3,3}$ was not statistically significant ($P = .108$).

The analysis of the pruned versions of the clinical galactograms showed an average root-mean-square fractional difference between the original R-matrix elements and the elements averaged over all pruned trees of 9.7% for all NF and RF galactograms (6.5% for the NF cases and 12.6% for the RF cases). A similar analysis, which considered 1,000 synthetically generated random binary trees pruned in the same fashion, yielded an average root-mean-square fractional difference of 6.8% (24).

DISCUSSION

We investigated the branching structure of ducts visualized on galactograms and evaluated the use of R matrices to classify galactographic findings. As an illustration of the classification results, Figure 4 shows two galactograms from the sets of NF and RF cases used in the study. The NF galactogram in Figure 4a corresponds to the values $r_{3,2} = 0.5$ and $r_{3,3} = 0.19$. The RF galactogram in Figure 4b corresponds to the values $r_{3,2} = 0.33$ and $r_{3,3} = 0.67$.

Results obtained in this study show that element $r_{3,2}$ is approximately 50% smaller and element $r_{3,3}$ is approximately 50% larger when averaged over all RF images, relative to the average over NF images: $<r^{RF}_{3,2}> = 0.20$ whereas $<r^{NF}_{3,2}> = 0.38$, and $<r^{RF}_{3,3}> = 0.52$ whereas $<r^{NF}_{3,3}> = 0.33$. These differences in the matrix elements may be due to long-term processes that alter the ductal branching pattern. Another explanation may be cutoff or dilation of the ducts, which affects the filling of the ductal network with contrast agent and the visibility of the

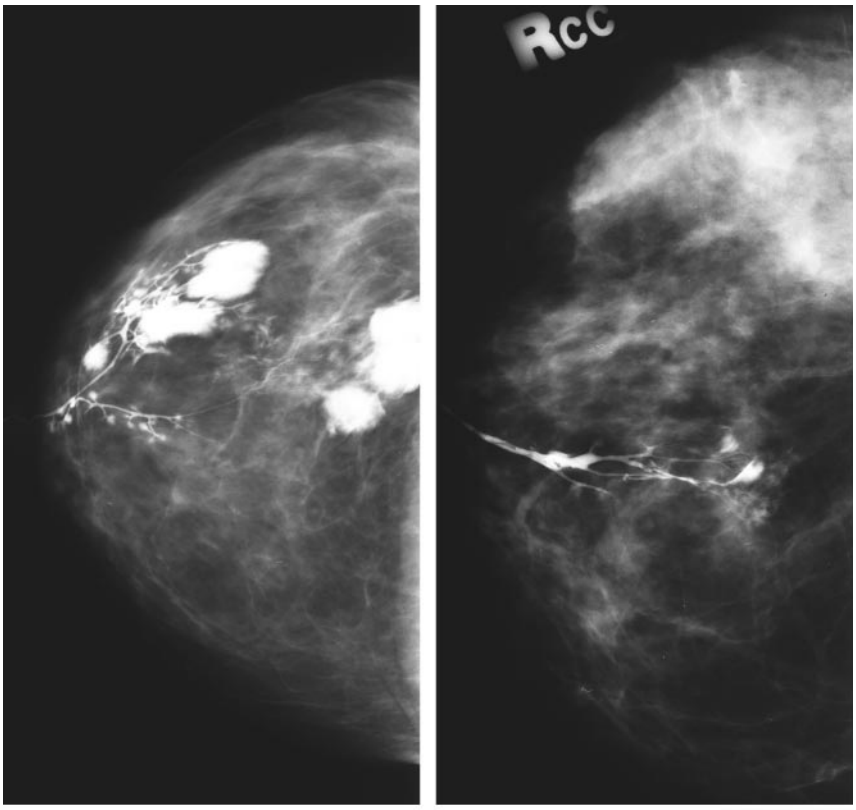

Figure 4. Two examples of galactograms that have been correctly classified by means of R matrices. **(a)** Galactogram with no reported findings (patient age, 45 years; right CC view; $r_{3,2} = 0.5$ and $r_{3,3} = 0.19$). (Large bright regions seen in this galactogram are due to extravasation, which did not affect the segmentation of the ductal tree.) **(b)** Galactogram with a reported finding of cysts (patient age, 55 years; right CC view; $r_{3,2} = 0.33$ and $r_{3,3} = 0.67$).

smaller ducts, thereby altering the calculated R matrix. Further research is needed to investigate the relationship between galactographic changes and R-matrix element values.

The root-mean-square fractional difference, estimated from analysis of the pruned ductal trees, is on average 9.7%, significantly smaller than the difference between the average values of matrix elements $r_{3,2}$ and $r_{3,3}$. Moreover, the sample standard deviation of these elements is significantly larger than the root-mean-square difference measured from pruning. The means and standard deviations of these elements are shown in Figure 2. These findings substantiate the robustness of the R-matrix representation of ductal networks, as the observed variation in the galactograms cannot be explained by the accuracy of the segmentation.

Evaluation with the simulated data showed that classification based on a single element, $r_{3,3}$, performs at a statistically significant level ($P = .007$). The performance of classification based on a pair of elements, $r_{3,2}$ and $r_{3,3}$, was not significant ($P = .108$). This reduction in significance is understandable given that the use of two matrix elements increases the probability that some pair will give a spuriously efficacious classification and given that the classifier design assigned equal importance to each matrix element to avoid overspecification.

Several confounding factors should be considered in the interpretation of these results. Patient age distributions differ for the NF and RF cases (mean age, 44.2 years for NF vs 54.8 years for RF). We tested and found essentially no correlation between the age and the matrix element values, with Pearson correlation coefficient values of 0.18 and 0.01 for the elements $r_{3,2}$ and $r_{3,3}$, respectively. Another possible influence could be our combination of galactograms obtained with all views, CC and ML/MLO. In an ideal case, with all the branches visible and with perfect segmentation, the reconstructed ductal trees would be the same on both CC and ML/MLO views, as would the corresponding R matrices, which was not the case in this experiment. We compared the maximum difference between the mean element values computed over normal and benign galactograms with the maximum difference between the mean element values computed over CC and ML/MLO views and found the former difference approximately two times greater than

the latter. The most limiting factor in our study, however, was the small sample.

In summary, our preliminary analysis indicates that R matrices may be used to identify cases with reported galactographic findings. The performance of classification with a single matrix element was statistically significant in a set of eight NF cases (12 views) and seven RF cases (13 views) with findings of ductal ectasia, cysts, or papilloma. Further experiments should use more galactograms and a more sophisticated decision rule and should include malignant cases.

REFERENCES

1. Kopans DB. Breast imaging. 2nd ed. Philadelphia, Pa: Lippincott-Raven, 1998.
2. Lanyi M. Diagnosis and differential diagnosis of breast calcifications. Berlin, Germany: Springer-Verlag, 1988.
3. Cooper AP. On the anatomy of the breast. London, England: Longman, 1840.
4. Dabelow A. Die milchdruese. In: Bargmann W, ed. Handbuch der mikroskopischen anatomie des menschen: haut und sinnesorgane. Berlin, Germany: Springer-Verlag, 1957; 277–485.
5. Egan RL. Breast imaging: diagnosis and morphology of breast diseases. Philadelphia, Pa: Saunders, 1988.
6. Bland KI, Copeland EM III, eds. The breast: comprehensive management of benign and malignant diseases. 2nd ed. Philadelphia, Pa: Saunders, 1998.
7. Gregl A. Color atlas of galactography: clinical and radiological symptomatology and therapy of the secreting breast. Stuttgart, Germany: Schautter, 1980.
8. Tabar L, Dean PB, Pentek Z. Galactography: the diagnostic procedure of choice for nipple discharge. Radiology 1983; 149:31–38.
9. Cardenosa G, Doudna C, Eklund GW. Ductography of the breast: technique and findings. AJR Am J Roentgenol 1994; 162:1081–1087.
10. Dinkel HP, Trusen A, Gassel AM, et al. Predictive value of galactographic patterns in benign and malignant neoplasms of the breast in patients with nipple discharge. Br J Radiol 2000; 73:706–714.
11. Sauter ER, Ehya H, Babb J, et al. Biologic markers of risk in nipple aspirate fluid are associated with residual cancer and tumor size. Br J Cancer 1999; 81:1222–1227.
12. Wolfe JN. Risk for breast cancer development determined by mammographic parenchymal patterns. Cancer 1976; 37:2486–2492.
13. Moffat DF, Going JJ. Three dimensional anatomy of complete duct systems in human breast: pathological and developmental implications. J Clin Pathol 1996; 49:48–52.
14. Ohtake T, Abe R, Kimijima I, et al. Intraductal extension of primary invasive breast carcinoma treated by breast-conservative surgery: computer graphic three-dimensional reconstruction of the mammary duct-lobular systems. Cancer 1996; 76:32–45.
15. Taylor P, Owens R, Ingram D. Simulated mammography using synthetic 3D breasts. In: Karssemeijer N, Thijssen M, Hendriks J, van Erning L, eds. Digital mammography: Nijmegen, 1998. Dordrecht, the Netherlands: Kluwer Academic, 1998; 283–290.
16. Bakic PR. Breast tissue description and modeling in mammography. Dissertation. Lehigh University, Bethlehem, Pa, 2000.
17. Viennot XG, Eyrolles G, Janey N, Arques D. Combinatorial analysis of ramified patterns and computer imagery of trees. Comput Graph 1989; 23:31–40.
18. Humphreys RC, Lydon J, O'Malley BW, Rosen JM. Mammary gland development is mediated by both stromal and epithelial progesterone receptors. Mol Endocrinol 1997; 11:801–807.
19. Atwood CS, Hovey RC, Glover JP, et al. Progesterone induces side-branching of the ductal epithelium in the mammary glands of peripubertal mice. J Endocrinol 2000; 167:39–52.
20. Russo IH, Russo J. Role of hormones in mammary cancer initiation and progression. J Mammary Gland Biol Neoplasia 1998; 3:49–61.
21. Hansen RK, Bissell MJ. Tissue architecture and breast cancer: the role of extracellular matrix and steroid hormones. Endocr Relat Cancer 2000; 7:95–113.
22. Brisken C. Hormonal control of alveolar development and its implications for breast carcinogenesis. J Mammary Gland Biol Neoplasia 2002; 7:39–48.
23. Efron B. The jackknife, the bootstrap and other resampling plans. Philadelphia, Pa: Society for Industrial and Applied Mathematics, 1982.
24. Bakic PR, Albert M, Maidment ADA. Evaluation of breast ductal networks using ramification matrices. In: Peitgen, HO, ed. Digital mammography. Heidelberg, Germany: Springer-Verlag (in press).